Journal of Hazardous Materials 161 (2009) 175–182

Contents lists available at ScienceDirect

Journal of Hazardous Materials

journal homepage: www.elsevier.com/locate/jhazmat

Preparation and application of nanoglued binary titania–silica aerogel

Liang Luo [a], Adrienne T. Cooper [a,*], Maohong Fan [b]

[a] Department of Civil and Environmental Engineering, Temple University, 1947 North 12th Street, Philadelphia, PA 19122, United States
[b] College of Materials Science and Engineering, Georgia Institute of Technology, 771 Ferst Drive, Atlanta, GA 30332, United States

ARTICLE INFO

Article history:
Received 27 May 2007
Received in revised form 10 December 2007
Accepted 13 March 2008
Available online 30 March 2008

Keywords:
Binary aerogel
Silica matrix
Photocatalysis
Reaction kinetics
Hydroxyl radical

ABSTRACT

Nanoglued binary titania (TiO_2)–silica (SiO_2) aerogel, as a novel type of photocatalyst, has been synthesized on glass substrates. Using an about-to-gel SiO_2 sol as nanoglue, anatase TiO_2 aerogel was immobilized into a three-dimensional mesoporous network of the SiO_2. Factorial designs were employed to optimize both TiO_2 aerogel and binary TiO_2–SiO_2 aerogel synthesis. Characterization of the as-prepared TiO_2 and binary samples by surface area, porosity, and surface chemical composition showed that the photocatalysts were high-surface-area nanoporous materials, with a Ti^{4+} valency. The binary aerogel exhibited high photocatalytic activity for the degradation of methylene blue (MB) under simulated solar light; the reaction followed the pseudo first-order Langmuir–Hinshelwood (L–H) kinetic model. Fluorescence spectroscopy revealed that the hydroxyl ($^{\bullet}OH$) radical was formed during the illumination of the binary TiO_2–SiO_2 aerogel in a solution of probe molecules, which corroborates the probable mechanism of hydroxyl radical oxidation of contaminants in photocatalytic reactions.

1. Introduction

Due to its high photocatalytic activity and chemical stability, titanium dioxide (TiO_2) has been extensively investigated as a photocatalyst for environmental remediation [1–3]. Effective degradation of a range of contaminants using TiO_2 photocatalysis has been demonstrated at the bench-scale [3–13]. However, two issues, improvement of photocatalytic efficiency and recovery–reuse of the catalyst [3,14], need to be resolved before the application of TiO_2 photocatalysis is practical on a large scale. TiO_2 photocatalytic efficiency can be improved by increasing the surface area available to adsorption of contaminants and enhancing access of reactants to reactive sites. For better recovery and reuse, TiO_2 can be prepared in immobilized forms.

As a strategy to meet these needs, TiO_2 has been combined with other components to form composite photocatalysts. In many cases, SiO_2 is used as the second component for synthesizing binary TiO_2 materials. The binary TiO_2–SiO_2 materials have higher photocatalytic activity than traditional TiO_2 and are relatively easy to recover after use [7,14]. The photocatalytic superiority of composite TiO_2–SiO_2 over traditional TiO_2 is due to several characteristics. SiO_2, acts as a charge transfer catalyst (CTC), rapidly transferring photogenerated electrons and holes (e^-_{cb} and h^+_{vb}) to the solution or to surface ligand species before they recombine, improving the photocatalytic activity of TiO_2 [15]. In addition, because photocatalytic reactions usually take place at the interface of the catalyst, the higher the surface area of the photocatalyst, the greater the adsorption of reactants and the more likelihood the desired reactions will take place. The incorporation of TiO_2 into the matrix of a high surface area adsorbent such as SiO_2 will significantly increase the concentration of reactants near the active sites of TiO_2. Consequently, it will improve the probability of adsorption of the reactants [14,16]. The mesoporous structure of SiO_2 aerogel also allows easy access of reactants to the active center of TiO_2, which further enhances the photocatalytic reactions. Moreover, the Ti–O–Si bond formed in composite TiO_2–SiO_2 increases the band gap energy of the active center of TiO_2 [17]. The higher the band gap energy of TiO_2, the higher the oxidizing potential of the photogenerated holes (h^+_{vb}), and the higher the reducing potential of the electrons (e^-_{cb}), leading to greater photocatalytic activity of TiO_2.

Conventional composite material synthesis is based on three primary techniques: (1) incorporating the guest component into the silica (SiO_2) structure at the stage of formation of silicon precursor [18–20]; (2) impregnating precursors of the selected guest components into the already formed host's solid networks in which the precursors could react to form active centers [21]; and (3) using silica as a template for the guest components for synthesizing materials with new crystalline structures [22].

The present research examines a new synthesis method for composite binary photocatalyst. Specifically, the immobilization of the binary TiO_2–SiO_2 aerogel onto a glass substrate has been realized by incorporating the photocatalytic guest TiO_2 aerogel

* Corresponding author. Tel.: +1 215 204 7802; fax: +1 215 204 4696.
E-mail address: acooper@temple.edu (A.T. Cooper).

0304-3894/$ – see front matter © 2008 Elsevier B.V. All rights reserved.
doi:10.1016/j.jhazmat.2008.03.105

Table 1
Assignment of factors and levels for the 2 × 3 full factorial design

	Trial no.								
	1	2	3	4	5	6	7	8	9
Soaking time (min)	10	10	10	20	20	20	30	30	30
Extraction rate (L/min)	0.25	0.50	0.75	0.25	0.50	0.75	0.25	0.50	0.75

into the host-silica sol only minutes prior to the gelation of silica sol. This timing minimizes the interaction time between the silica colloids and the guest, and prevents total encapsulation of TiO_2 by silica that results in interruption of transport paths in the synthesized composite aerogel [23]. Immobilization onto glass alleviates the catalyst-recovery problem. Our previous study on "nanoglued" binary aerogel showed its effectiveness in degrading *Escherichia coli* and concluded that the mechanism of destruction was affected by the active center TiO_2 and catalyst surface area [24]. In this paper, we focus on the optimization of our "nanoglued" binary TiO_2–SiO_2 aerogel, testing its photocatalytic efficiency with an azo-dye, methylene blue (MB).

2. Materials and methods

2.1. Preparation of materials

Acetone, anhydrous ethanol, anhydrous methanol, coumarin, hydrochloric acid (0.1N), isopropanol, 70% nitric acid, tetramethoxysilane, terephthalic acid, and titanium (IV) isopropoxide were all purchased from Fisher Scientific (Pittsburgh, PA). Ammonia hydroxide (28% in H_2O) was obtained from Sigma–Aldrich (St. Louis, MO). Siphon bone-dry liquid carbon dioxide (CO_2) was purchased from Airgas (Philadelphia, PA). Deionized water used during the research was collected from a NANOpure® DIamond™ Life Science (UV/UF) ultrapure water system (Model D11931, Barnstead|Thermolyne, Dubuque, IA).

The nanoglued TiO_2–SiO_2 aerogel was synthesized in two steps, the preparation of TiO_2 aerogel and incorporation of the TiO_2 aerogel into a silica matrix [24]. The procedure of Pietron and Rolison [25] for preparation was modified to synthesize the nanoglued TiO_2–SiO_2 aerogel photocatalyst used in this research. The modifications include: (1) the change of molar ratio of titanium isopropoxide:nitric acid:ethanol:water in preparing TiO_2 gels to 1:0.08:20:3 based on the work of Degan and Tomkiewicz [26], where it was reported that this specific ratio would produce the most stable and porous titania (TiO_2) aerogel; and, (2) the adoption of an acid-catalyzed and base-catalyzed sol–gel method in preparing the about-to-gel silica sol in lieu of the solely base-catalyzed sol–gel method. The advantage of the two-catalyst method is the ability to control the network microstructure of the aerogel [27]. A Polaron CPD 7501 critical point dryer (Energy Beam Sciences, Agawarm, MA) was used to convert gel into aerogel. A vacuum oven (Yamato ADP-21, Yamato Scientific America Inc., Santa Clara, CA) and a muffle furnace (Fisher Scientific Isotemp® Programmable, Springfield, NJ) were used for thermal processing of the TiO_2.

2.1.1. TiO_2 aerogel preparation optimization

A full factorial design (2 × 3) was chosen to optimize the TiO_2 aerogel preparation. In our previous research, it was observed that soaking time and extraction rate during the CO_2 supercritical drying treatment were likely to affect the final surface area of TiO_2 aerogel [24]. Therefore, these two factors were designated as investigative variables. The assignment of factors and levels are shown in Table 1. Three replicate surface area measurements were obtained for each combination.

2.1.2. TiO_2–SiO_2 binary aerogel preparation

TiO_2 aerogel with the highest surface area based on the optimization described in Section 2.1.1 was nanoglued using the about-to-gel silica sol onto a 1 cm × 1 cm glass substrate. In addition to soaking and extraction times, two other factors were considered for optimization of the binary aerogel, acid–base ratio and mass of as-optimized titania, which made a full factorial design impractical. Therefore, Taguchi's L_9 $(3)^4$ orthogonal array design (OAD) [28,29], as shown in Table 2, was used to identify the optimum conditions for preparation of the binary sample with the highest photocatalytic activity.

2.2. Characterization of materials

The surface area, pore size, and pore volume of the TiO_2 aerogel and binary TiO_2–SiO_2 aerogel were measured using an ASAP 2020 accelerated surface area and porosimetry analyzer (Micromeritics, Norcross, GA). XPS data were acquired with unmonochromatized Mg Kα radiation at 1253.6 eV using a Physical Electronics source controller (Model 32-095, RBD Enterprise, Bend, Oregon) and a vacuum chamber with a base pressure of 1×10^{-9} torr. A hemispherical analyzer (VG100AX, VG Microtech, East Sussex, UK) was used to obtain the energy distribution of the photoemitted electrons. A pass energy of 75 eV was used for survey scans and 25 eV was used for all other spectra.

Table 2
Assignment of factors and levels for the L_9 (3^4) orthogonal array matrix, and corresponding photocatalytic removal ratio of methylene blue

Trial no.	Factors				
	Soaking time (min)	Extraction rate (L/min)	Titania mass (mg/cm^2)	V_{HCl} : V_{NH_4OH} (μL:μL)	Removal ratio (%)
1	10	0.25	10	0:125	81.6
2	10	0.50	15	120:125	60.9
3	10	0.75	20	60:125	71.2
4	20	0.25	15	60:125	63.1
5	20	0.50	20	0:125	66.3
6	20	0.75	10	120:125	73.7
7	30	0.25	20	120:125	75.3
8	30	0.50	10	60:125	94.3
9	30	0.75	15	0:125	81.2

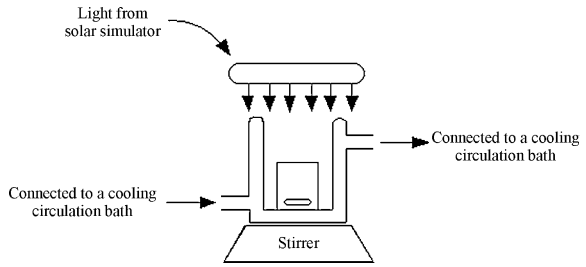

Fig. 1. Photocatalytic experimental setup for degradation of methylene blue.

2.3. Photocatalytic degradation of methylene blue

The photocatalytic degradation of methylene blue was conducted in a batch reactor under a solar simulator (1000 W Oriel Solar Simulators, Newport Corporation, Irvine, CA), as shown in Fig. 1. The cylindrical reactor has a height of 10.16 cm (4 in.), inner diameter of 7.62 cm (3 in.) and outer diameter of 5.08 cm (2 in.), and was placed 10 cm from the light source. A rack was used to hold the catalyst in the middle of the reactor, where the irradiation intensity was measured at 132.7 mW/cm^2. Under the rack, a magnetic stirring bar was used to maintain a well-mixed reaction condition. Two segments of Tygon® tubing were used to connect the reactor to a digital cooling circulation bath (RC20 CS Lauda, Brinkmann, Westbury, NY) to maintain the reaction temperature at 20 °C. For each 2-h experimental run, the methylene blue solution was placed into the reactor at an initial concentration of 4 mg/L, and the entire reactor was placed under a the solar simulator; external light was blocked by covering the solar simulator and the reactor with opaque boards.

Samples were taken at 15, 30, 45, 60, 90, and 120 min, and concentration was measured by a spectrophotometer (DR/4000U, HACH Company, Loveland, CO) at an absorption peak of 664 nm. Experimental controls consisted of a dark reactor and a reactor with no catalyst (but exposed to light) for each experimental combination. Three replicates were performed for each of the nine trials.

2.3.1. Reaction kinetics

For evaluation of photocatalytic activity, binary TiO_2–SiO_2 aerogel immobilized on the glass substrate was prepared under the optimum condition identified using the orthogonal array design analysis and described in Section 2.1.2. These as-prepared composite samples were used to confirm the validity of the OAD design and study the reaction kinetics of methylene blue removal. Using the same procedure as that identified in Section 2.3, the concentration of methylene blue was measured over a 2-h period, at intervals of 15 min for the first hour and 30 min for the second hour. The reaction order and reaction rate constant for both photocatalytic and photolytic degradation of methylene blue were obtained graphically from the relationship between natural logarithm of the normalized concentration, $\ln(C_0/C)$, and reaction time.

2.3.2. Reaction mechanism and hydroxyl radical detection

In TiO_2 photocatalysis, active oxygen species such as hydroxyl radical (•OH), superoxide radical ($O_2^{\bullet -}$), perhydroxyl radical (•OOH) and hydrogen peroxide (H_2O_2) have been regarded as the key species to degrade contaminants. Among these highly oxidative species, the hydroxyl radical (•OH) has long been assumed to be the major species for mineralization of pollutants either adsorbed on the TiO_2 surface or in the bulk solution [30,31]. The degradation of methylene blue has also been assumed to follow the reaction mechanism of hydroxyl oxidation. Coumarin and terephthalic acid were used as probe molecules to validate the appearance of hydroxyl radical in the photocatalytic degradation of methylene blue with our binary TiO_2–SiO_2 aerogel [32]. Coumarin and terephthalic acid react with •OH to form the highly fluorescent intermediates, 7-hydroxycoumarin [32–35] and 2-hydroxyterephthalic acid [32,36–40] as shown in Figs. 2 and 3. A Fluoromax-2® spectrofluorometer (ISA/JOBIN YVON-SPEX, Edison, NJ) was used to obtain the emission fluorescence spectra for both 7-hydroxycoumarin and 2-hydroxyterephthalic acid. The 7-hydroxycoumarin was scanned with an excitation at 332 nm, starting at 342 nm and ending at 650 nm. The 2-hydroxyterephthalic acid was scanned with an excitation at 315 nm, starting at 325 nm and ending at 620 nm. Both scans were performed at an increment of 1 nm and with an integration time of 0.10 s. The final results were generated based upon the average of three scans.

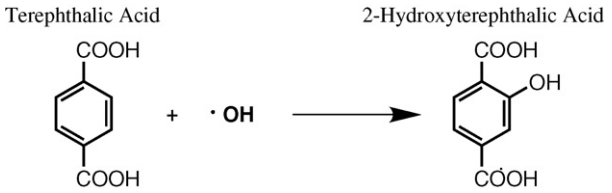

Fig. 2. Reaction of terephthalic acid with hydroxyl radical to form fluorescent 2-hydroxyterephtalic acid.

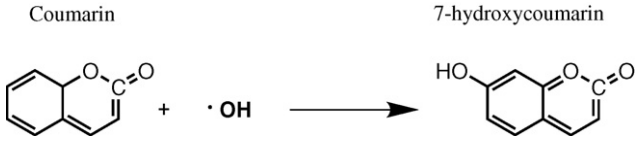

Fig. 3. Reaction of coumarin with hydroxyl radical to form fluorescent 2-hydroxycoumarin.

3. Results and discussion

3.1. Factors affecting the quality of TiO_2 aerogel

In this study, the technique of CO_2 supercritical drying was used to prepare a highly porous TiO_2 aerogel that possesses much higher surface area than other forms [1–3,14]. Factors such as soaking time and extraction rate during supercritical drying are believed to affect the crystalline structure and surface area of TiO_2 [24]. The experimental results from our 2×3 factorial design corroborate this assertion. From Fig. 4, there is an apparent trend of increasing surface area with soaking time in liquid CO_2, from 10 min to 20 min, followed by a slight decrease from 20 min to 30 min. However, the surface area for both 20 min and 30 min are higher than those at 10 min. The increase from 10 min to 20 min is likely due to a need for the aerogel to have sufficient soaking time in liquid CO_2 to allow for replacement of the acetone in the TiO_2 crystalline grid. However, increasing extraction rate also has an effect on surface area. A CO_2 extraction rate of 0.75 L/min, the fastest rate tested, yields the highest surface area achieved in this study. The optimum preparation conditions are selected based on the samples with the highest surface area, as shown in Fig. 4: a soaking time of 20 min or 30 min and extraction rate of 0.75 L/min. The variability in the data, particularly at the slower extraction rates, is likely due to errors introduced from manual extraction rate control during the supercritical drying process. Additionally, the aerogel preparation process takes place over an 8-day period, increasing the probability of humidity effect and operational error.

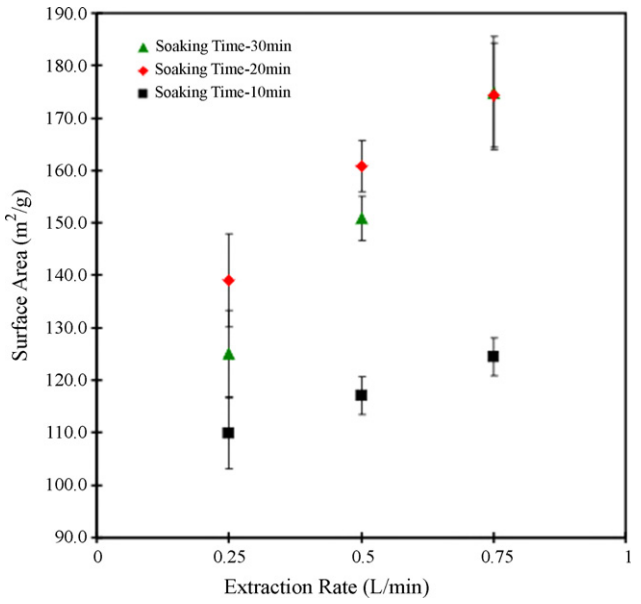

Fig. 4. TiO_2 aerogel surface area as a function of extraction rate and soaking time.

Table 3
Analytical results of the L_9 (3^4) orthogonal array design

	$Factor_{level}$			
	Soaking time	Extraction rate	Titania mass	$M_{HCl} : M_{NH_4OH}$
K_1	213.7	220	249.6	229.1
K_2	203.1	221.5	205.2	209.9
K_3	250.8	226.1	212.8	228.6
k_1	71.233	73.333	83.200	76.367
k_2	67.700	73.833	68.400	69.967
k_3	83.600	75.367	70.933	76.200
R	15.900	2.033	14.800	6.400

3.2. Factors affecting the preparation of binary aerogel

Photocatalytic degradation of methylene blue was used to investigate the photocatalytic activity of TiO_2–SiO_2 binary aerogel prepared in each of the nine experimental trials in the L_9 (3^4) orthogonal array design (Table 2). Factors evaluated using this design were the soaking time and extraction rate of the supercritical drying stage, the mass of titania, and the acid–base ratio in the silica gelation process, each of which has three different levels, as shown in Table 2. The removal ratio of methylene blue at 60 min was selected as the response. TiO_2 aerogel for this study was prepared under the optimum conditions reported in Section 3.1, a soaking time of 20 min and an extraction rate of 0.75 L/min.

The results in Table 2 show that the samples prepared from trial eight had the highest photocatalytic activity, with an average methylene blue removal ratio of 94.3% at 60 min. This corresponds to a soaking time of 30 min, extraction rate of 0.50 L/min, titania mass of 10 mg/cm^2, and an acid–base volumetric ratio of 60:125 (molar ratio: 0.00667).

Table 4
Analysis of variance (ANOVA) results of the L_9 (3^4) orthogonal array design

	Factor				
	SS	DF	F values	F (critical)	Significance
Soaking time	418.229	2	62.089	19.000	*
Extraction rate	6.736	2	1.000	19.000	
Titania mass	375.929	2	55.809	19.000	*
Acid–base ratio	79.842	2	11.853	19.000	
Error	6.736	2			

The asterisk indicates that the factor is significant because the F-value is greater than F-critical.

Statistical analysis of the data indicates that the optimal combination corresponds to a soaking time of 30 min, extraction rate of 0.75 L/min, titania mass of 10 mg/cm^2, and $V_{HCl} : V_{NH_4OH}$ of 0:125 (acid-free). These results are provided in Table 3, where K_n is the sum of results at n level, k_n denotes K_n/3, and R is the range k values. The highest k value for a given factor corresponds to the optimal level for that factor. The R values provide information on the relative importance of the factors; the larger the range the more important the factor. In our study, soaking time was the most important factor, followed by titania mass and acid–base ratio, with extraction rate being the least important.

Results of the analysis of variance (ANOVA) are shown in Table 4. The small range, R value, for extraction rate compared to that of the other factors, indicates that it has the least significance on the efficacy of the binary aerogel; therefore the extraction rate was chosen as the error source. Based on the F values, soaking time and titania mass are statistically significant. On the other hand there is little difference between levels for extraction rate and acid–base ratio. Considering statistically significant factors first, the experimentally identified optimum conditions for preparation of the binary aerogel are a reasonable selection.

3.3. Characteristics of TiO_2 and TiO_2–SiO_2

3.3.1. Surface area and porosity analysis

The surface area and porosity of TiO_2 aerogel was analyzed using an ASAP® 2020 accelerated surface area and porosimetry system. Fig. 5 shows the nitrogen adsorption–desorption isotherms (upper curves) for a TiO_2 aerogel sample with a surface area of 182.6 m^2/g prepared using the optimum combination, 20 min soaking time and 0.75 L/min extraction rate. The second (lower curves) isotherm shown in Fig. 5 is of a TiO_2 aerogel sample with a surface area of 123.5 m^2/g prepared using sub-optimum conditions, a soaking time of 10 min and extraction rate of 0.75 L/min. Both demonstrate characteristics of the Type IV IUPAC isotherm classification, which is associated with the existence of mesoporosity [41]. Comparing these two isotherms, it is seen that the hysteresis loop

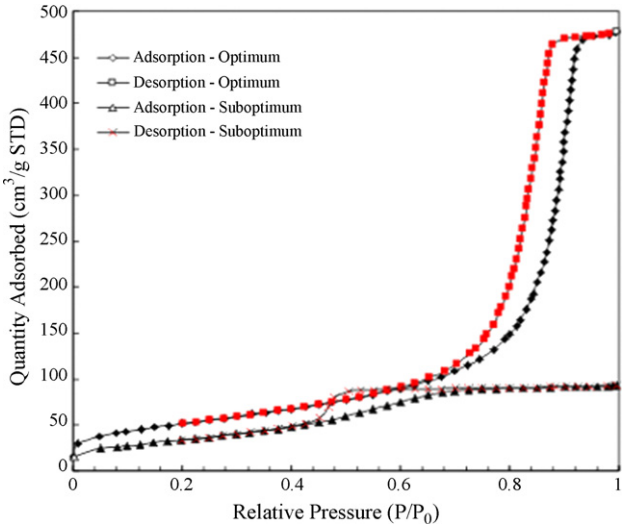

Fig. 5. Adsorption and desorption isotherm for a TiO_2 aerogel prepared under optimum conditions: soaking time of 20 min and CO_2 extraction rate of 0.75 L/min, and sub-optimum conditions: soaking time of 10 min and CO_2 extraction rate of 0.75 L/min.

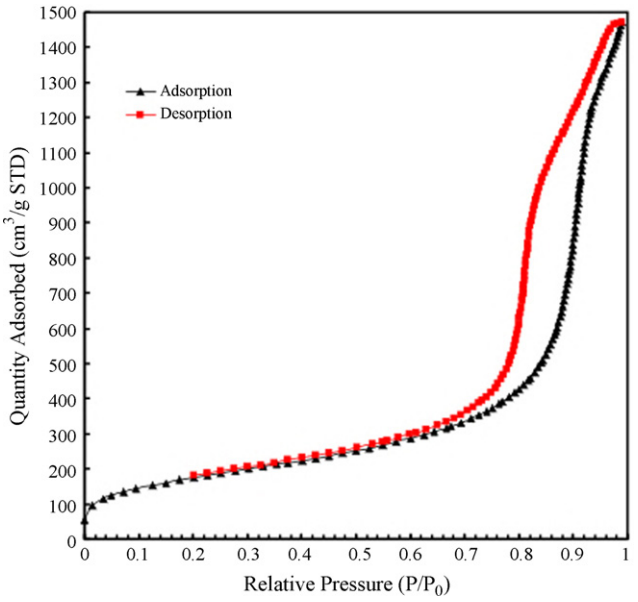

Fig. 6. Adsorption and desorption isotherm for an optimized binary TiO_2–SiO_2 sample.

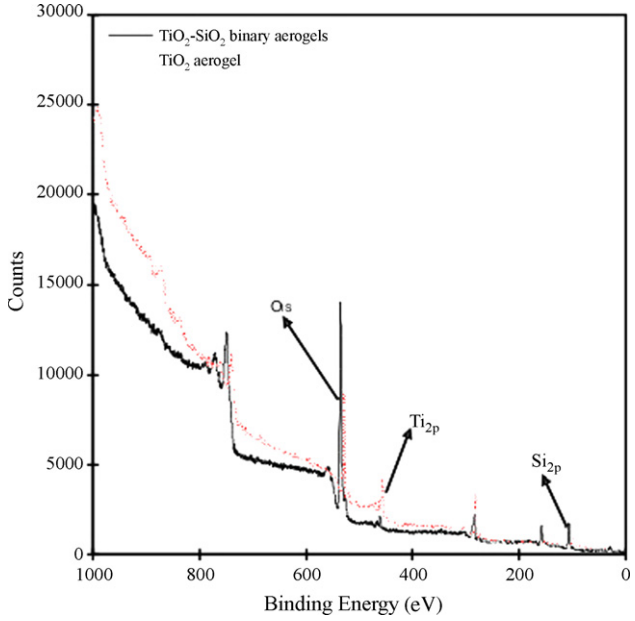

Fig. 7. XPS survey scan of optimum TiO_2 aerogel and binary TiO_2–SiO_2 aerogel.

for the sample with the higher surface area (the upper isotherm) is much narrower than that of the lower surface area sample (the lower isotherm) and appears at high relative pressure (p/p^0) values. This feature indicates that the capillary condensation only takes place between particles and that virtually no intraparticle mesoporosity exists in this sample [42]. Additionally, BET analysis of the isotherm data indicates that the higher surface area sample (the upper isotherm) has a larger pore volume, 0.74 cm^3/g, than that of the lower surface area sample (the lower isotherm), which has a pore volume of 0.145 cm^3/g. The average pore widths are 16.2 nm and 4.7 nm, respectively, for the higher surface area and lower surface area samples. Generally, the ratio of pore volume to pore size is reflective of the surface area of a sample.

Fig. 6 gives the nitrogen adsorption–desorption isotherm for an optimized binary TiO_2–SiO_2 sample, which was prepared using a soaking time of 30 min, extraction rate of 0.75 L/min, titania mass of 10 mg/cm^2, and V_{HCl} : V_{NH_4OH} of 0:125. The optimized binary sample has a surface area of 620.3 m^2/g, a pore volume of 2.28 cm^3/g and an average pore size of 14.7 nm. The binary sample's high surface area is believed to be responsible for its efficacy for the degradation of methylene blue.

By comparing the ordinate axis of all three isotherms, it can be observed that with the increase of sample surface area, greater quantities of nitrogen have been adsorbed. The binary TiO_2–SiO_2 aerogel with the highest surface area adsorbed the most nitrogen. This fact could lead to the probability that binary samples will adsorb more contaminants onto the surface during photocatalytic reaction, and thus have a higher chance of degradation, than using TiO_2 alone.

3.4. X-ray photoelectron spectroscopy analysis

Chemical composition of sample surfaces can be identified by the survey scan spectra (intensity vs. binding energy/eV) for TiO_2 aerogel and binary TiO_2–SiO_2 aerogel, as shown in Fig. 7. Some shifting was observed between TiO_2 aerogel and binary aerogel. This phenomenon was attributed to the existence of the second component, SiO_2, which serves as an insulator and leads to charging.

The oxidation state of titanium can be assessed primarily based on the energy difference between 1/2 and 3/2 shells of titanium. Fig. 8 gives the shifting-corrected XPS analysis spectra of $Ti_{2p1/2}$ and $Ti_{2p3/2}$ for commercially standard Degussa TiO_2, optimum TiO_2 aerogel, and optimum binary TiO_2–SiO_2 aerogel. The energy splitting between $Ti_{2p1/2}$ and $Ti_{2p3/2}$ is 5.7 eV, which confirms the existence of Ti^{4+} compared to 6.15 eV for titanium metal.

3.5. Photocatalytic reaction kinetics and mechanism of methylene blue

3.5.1. Kinetics

The study of TiO_2 photocatalytic reaction kinetics is not only the basic requirement for design of cost-effective reactors for application, but also an approach to better understanding the reaction mechanism. Many researchers have proposed that the photocatalytic decontamination of a wide range of pollutants by

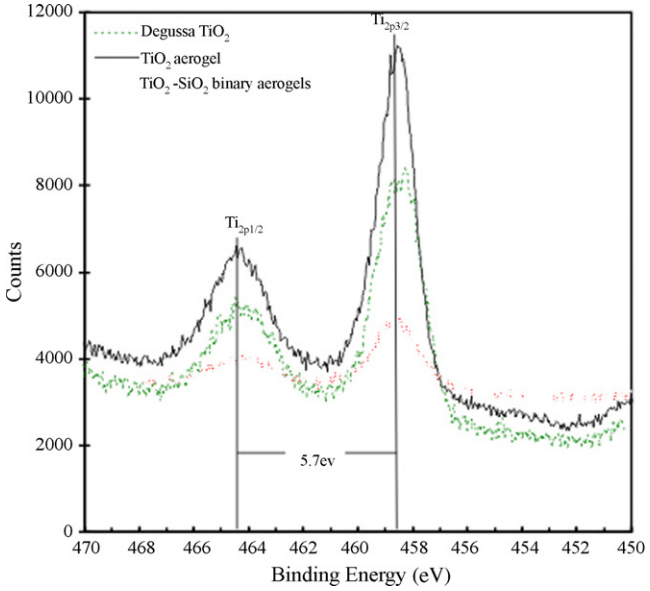

Fig. 8. Shifting-corrected XPS analysis spectra of $Ti_{2p1/2}$ and $Ti_{2p3/2}$ for Degussa TiO_2, optimum TiO_2 aerogel, and optimum binary TiO_2–SiO_2 aerogel.

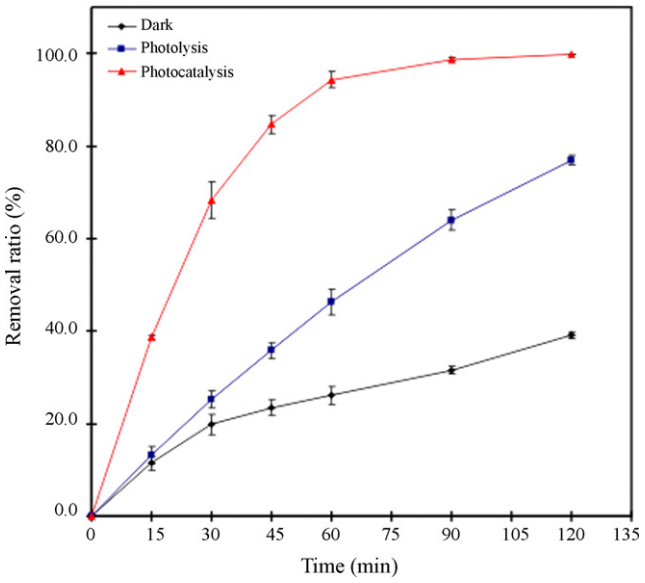

Fig. 9. Photocatalytic degradation of methylene blue by binary TiO_2–SiO_2 aerogel prepared using the optimum combination.

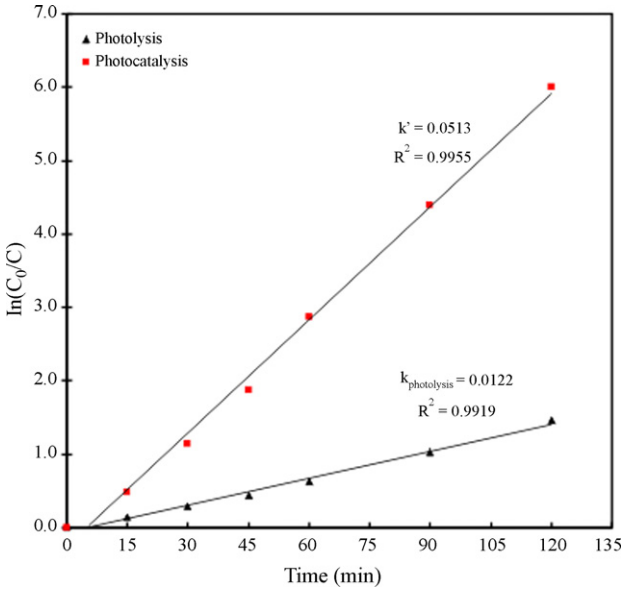

Fig. 10. Linearized relationship of $\ln(C_0/C)$ vs. time of binary sample prepared under the optimum combination of factors and levels.

TiO_2 follow the well-known Langmuir–Hinshelwood (L–H) kinetics model [9,10,14,43–46]. When this L–H model is applied to the immobilized TiO_2, some assumptions have to be made considering the possible involvement of the mass transport effects. Under the well-mixed transport condition, we assume that O_2 in the solution is always saturated, and that there is no difference between the interfacial concentration of contaminant and that in the bulk solution. Then, the rate law Eq. (1) can be expressed as

$$r = \frac{kKC}{1 + KC} \tag{1}$$

where C is the contaminant concentration, k is the apparent reaction rate constant, and K is the equilibrium adsorption constant of that contaminant. The kinetic constants, k and K can be calculated by taking the reciprocal of both sides of the reaction rate Eq. (1) to form the linear Eq. (2):

$$\frac{1}{r} = \frac{1}{kK}\frac{1}{C} + \frac{1}{k} \tag{2}$$

When the initial concentration of the contaminant, C_0 is small, integration of the Eq. (2) yields the simplified pseudo first-order reaction kinetics equation:

$$\ln\left(\frac{C_0}{C}\right) = kKt = k't \tag{3}$$

where k' is the apparent pseudo first-order reaction rate constant.

In this research, this pseudo first-order Langmuir–Hinshelwood kinetics model was assumed to be feasible for the photocatalytic degradation of methylene blue by the nanoglued TiO_2–SiO_2 binary aerogel. If this assumption is valid, plotting $\ln(C_0/C)$ vs. reaction time (t) will lead to a straight line whose slope equals the apparent pseudo first-order reaction rate constant, k'.

The removal of methylene blue under photocatalytic, photolytic, and dark conditions is graphically illustrated in Fig. 9. From the figure, it is clear that the photocatalytic degradation of methylene blue is much faster than the dark and photolytic reactions, and that the most degradation occurred by 60 min when the removal ratio reached around 95%. Under the dark condition, removal ratios of around 26% and 40% were achieved at 60 min and 90 min, respectively. This can be attributed to the high porosity of the binary TiO_2–SiO_2 aerogel, which correlates to a strong adsorption ability.

A graph of $\ln(C_0/C)$ vs. time yields a good linear relationship ($R^2 = 0.9955$) for photocatalytic degradation of MB, as shown in Fig. 10. This result consolidates the assumption that the degradation of MB by the nanoglued binary TiO_2–SiO_2 aerogel follows the pseudo first-order reaction kinetics, and can be represented by the simplified Langmuir–Hinshelwood model. The linearized plot ($R^2 = 0.9919$) for photolysis indicates that the photolytic degradation of MB is a simple first-order reaction. A comparison of the reaction rate constants of photocatalysis ($k' = 0.0513$) and photolysis ($k_{photolysis} = 0.0122$) also confirms that photocatalysis plays an important role in destruction of methylene blue.

3.6. Mechanism

Binary TiO_2–SiO_2 aerogels, prepared from the optimized procedure, were placed in a 1×10^{-3} M aqueous solution of coumarin and a 4×10^{-4} M NaOH solution of terephthalic acid. The two solutions with the binary photocatalyst, magnetically stirred, were illuminated with the simulated solar light (132.7 mW cm^{-2}). The fluorescence emission spectra excited at 332 nm from coumarin and at 315 nm from terephthalic acid were measured every 5 min of illumination and are shown in Figs. 11 and 12.

As seen in the figures, both show a gradual increase in fluorescence at 452 nm for coumarin and at 425 nm for terephthalic acid, under continuous illumination of the binary aerogel. No obvious fluorescence increase was seen when coumarin and terephthalic acid solution were illuminated without the binary photocatalyst. These findings suggest that the occurrence of fluorescence can be ascribed to the chemical reactions between the probe molecules and the hydroxyl radicals formed on the binary TiO_2–SiO_2 aerogel surface via photocatalytic reaction. There is another possibility that the fluorescent hydroxyl products are formed due to the direct reaction between photogenerated holes and probe molecules [47,48]. However, this is unlikely since unless the concentration of the probe molecules is high, in the range of 10^{-1}–10^{-2} M, aromatic compounds like coumarin and terephthalic acid are oxidized by the hydroxyl radical ($^{\bullet}OH$) more rapidly than photogenerated holes [48,49]. In this experiment, low concentrations of coumarin (1×10^{-3} M) and terephthalic acid (4×10^{-4} M)

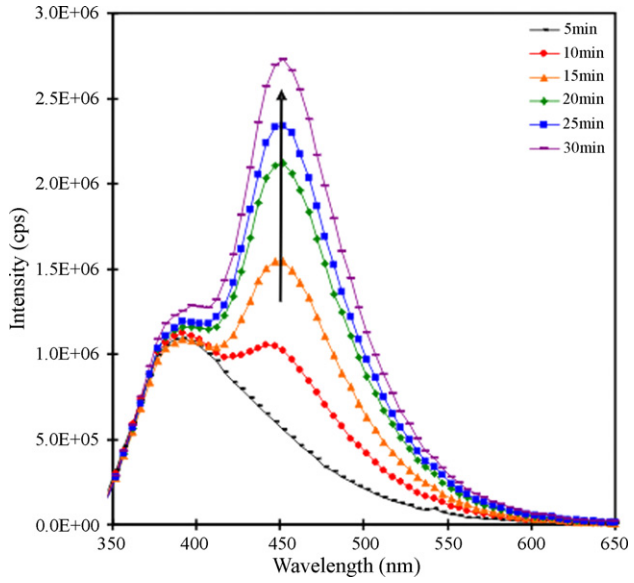

Fig. 11. Fluorescence spectral changes of 7-hydroxycoumarin observed at 5 min intervals during illumination of binary TiO_2–SiO_2 aerogel in 1×10^{-3} M aqueous solution of coumarin.

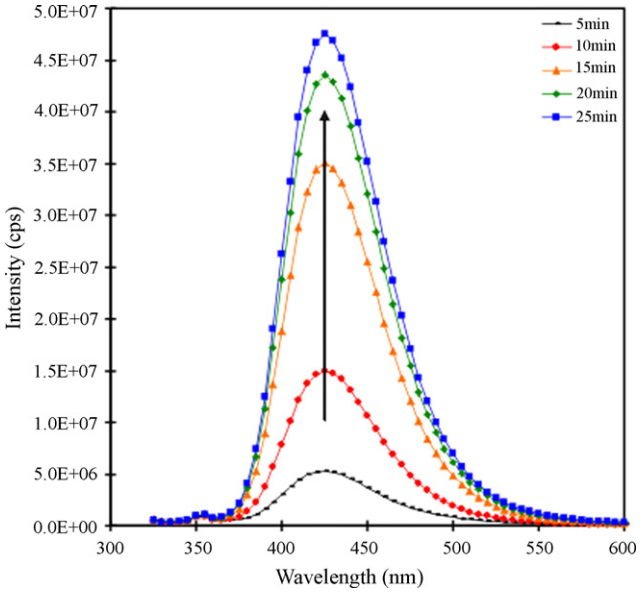

Fig. 12. Fluorescence spectral changes of 2-hydroxyterephthalic acid at 5 min intervals during illumination of binary TiO_2–SiO_2 aerogel in 4×10^{-4} M NaOH solution of terephthalic acid.

were used, indicating the production of 7-hydroxycoumarin and 2-hydroxyterephthalic acid. Based on previous reports in the literature [32–40], it is reasonable to assume that these fluorescent compounds result from the reaction between the probe molecules and •OH. The fluorescence analysis results further indicate that the photocatalytic destruction of contaminants by the nanoglued binary TiO_2–SiO_2 aerogel follows the assumed mechanism: generation of •OH during the photocatalytic reaction, and hydroxyl radical oxidation of contaminants.

4. Conclusions

A binary photocatalyst was prepared using a new two-step technique of nanogluing photocatalytically active TiO_2 aerogel into a three-dimensional network of SiO_2. The optimized nanoglued TiO_2–SiO_2 binary aerogel showed high photocatalytic activity in degradation of methylene blue. This result is attributed to the high surface area and porosity of the photocatalyst and existence of a strong adsorbent (SiO_2), which increase the concentration of methylene blue near the TiO_2 sites, thus enhancing the destruction efficiency. By using coumarin and terephthalic acid as probe molecules, fluorescence analysis of the hydroxylation products served as an effective method to examine the production of hydroxyl radicals (•OH) and substantiate the probable reaction mechanism of hydroxyl oxidation of pollutants in photocatalytic reactions.

Acknowledgements

This material is based upon work supported by the National Science Foundation under Grant No. BES-0401472. Any opinions, findings, and conclusions or recommendations expressed in this material are those of the authors and do not necessarily reflect the views of the National Science Foundation.

References

[1] M.R. Hoffmann, et al., Environmental applications of semiconductor photocatalysis, Chem. Rev. 95 (1) (1995) 69–96.
[2] A.L. Linsebigler, G.Q. Lu, J.T. Yates, Photocatalysis on TiO_2 surfaces—principles, mechanisms, and selected results, Chem. Rev. 95 (3) (1995) 735–758.
[3] R. van Grieken, et al., Synthesis of size-controlled silica-supported TiO_2 photocatalysts, J. Photochem. Photobiol. A: Chem. 148 (1–3) (2002) 315–322.
[4] S. Ahmed, T.J. Kemp, P.R. Unwin, Photomineralisation kinetics of aqueous chlorophenols at a supported TiO_2 surface studied by the channel-flow method with electrochemical detection, J. Photochem. Photobiol. A: Chem. 141 (1) (2001) 69–78.
[5] Z. Deng, et al., Preparation and photocatalytic activity of TiO_2–SiO_2 binary aerogels, Nanostruct. Mater. 11 (8) (1999) 1313–1318.
[6] S.H. Fan, et al., Photocatalytic degradation of cefradine in water over immobilized TiO_2 catalyst in continuous-flow reactor, Chin. J. Catal. 23 (2) (2002) 109–112.
[7] L.H. Gan, et al., Preparation of TiO_2/SiO_2 aerogels by non-supercritical drying method and their photocatalytic activity for degradation of pyridine, Chin. J. Chem. Eng. 13 (6) (2005) 758–763.
[8] N. Guettai, H.A. Amar, Photocatalytic oxidation of methyl orange in presence of titanium dioxide in aqueous suspension. Part II. Kinetics study, Desalination 185 (1–3) (2005) 439–448.
[9] C. Hu, et al., Photocatalytic degradation of cationic blue X-GRL adsorbed on TiO_2/SiO_2 photocatalyst, Appl. Catal. B: Environ. 40 (2) (2003) 131–140.
[10] O.E. Kartal, M. Erol, H. Oguz, Photocatalytic destruction of phenol by TiO_2 powders, Chem. Eng. Technol. 24 (6) (2001) 645–649.
[11] S.E. Park, H. Joo, J.W. Kang, Photodegradation of methyl tertiary butyl ether (MTBE) vapor with immobilized titanium dioxide, Sol. Energy Mater. Sol. Cells 80 (1) (2003) 73–84.
[12] C. Sahoo, A.K. Gupta, A. Pal, Photocatalytic degradation of methyl red dye in aqueous solutions under UV irradiation using Ag+ doped TiO_2, Desalination 181 (1–3) (2005) 91–100.
[13] G. Sivalingam, et al., Photocatalytic degradation of various dyes by combustion synthesized nano anatase TiO_2, Appl. Catal. B: Environ. 45 (1) (2003) 23–38.
[14] H.J. Kim, Y.G. Shul, H.S. Han, Photocatalytic properties of silica-supported TiO_2, Top. Catal. 35 (3/4) (2005) 287–293.
[15] C.S. Yang, C.J. Chen, Synthesis and characterization of silica-capped titania nanorods: an enhanced photocatalyst, Appl. Catal. A: Gen. 294 (1) (2005) 40–48.
[16] C. Anderson, A.J. Bard, An improved photocatalyst of TiO_2/SiO_2 prepared by a sol–gel synthesis, J. Phys. Chem. 99 (51) (1995) 17963–117963.
[17] X.T. Gao, I.E. Wachs, Titania–silica as catalysts: molecular structural characteristics and physico-chemical properties, Catal. Today 51 (2) (1999) 233–254.
[18] K. Fujiki, T. Ogasawara, N. Tsubokawa, Preparation of a silica gel carbon black composite by the sol gel process in the presence of polymer-grafted carbon black, J. Mater. Sci. 33 (7) (1998) 1871–1879.
[19] J. Wang, J. Kuhn, X. Lu, Monolithic silica aerogel insulation doped with TiO_2 powder and ceramic fibers, J. Non-Cryst. Solids 186 (1995) 296–300.
[20] C. Rutiser, S. Komarneni, R. Roy, Composite aerogels of silica and minerals of different morphologies, Mater. Lett. 19 (5–6) (1994) 221–224.
[21] G. Mitrikas, et al., Size distribution and EPR of silver nanoparticles in SiO_2 matrix, J. Non-Cryst. Solids 224 (1) (1998) 17–22.
[22] T.M. Tillotson, et al., Sol–gel processing of energetic materials, J. Non-Cryst. Solids 225 (1) (1998) 358–363.
[23] C.A. Morris, et al., Silica sol as a nanoglue: flexible synthesis of composite aerogels, Science 284 (5414) (1999) 622–624.

[24] J.M. Watson, A.T. Cooper, J.R.V. Flora, Nanoglued titanium dioxide aerogels for photocatalysis, Environ. Eng. Sci. 22 (5) (2005) 666–675.
[25] J.J. Pietron, D.R. Rolison, Electrochemically induced surface modification of titanols in a 'nanoglued' titania aerogel–silica aerogel composite film, J. Non-Cryst. Solids 285 (1–3) (2001) 13–21.
[26] G. Dagan, M. Tomkiewicz, TiO_2 aerogels for photocatalytic decontamination of aquatic environments, J. Phys. Chem. 97 (49) (1993) 12651–12655.
[27] T.M. Tillotson, L.W. Hrubesh, Transparent ultralow-density silica aerogels prepared by a 2-step sol–gel process, J. Non-Cryst. Solids 145 (1–3) (1992) 44–50.
[28] J.Y. Houng, et al., Applying the Taguchi robust design to the optimization of the asymmetric reduction of ethyl 4-chloro acetoacetate by bakers' yeast, J. Biotechnol. 100 (3) (2003) 239–250.
[29] W.G. Lan, et al., Orthogonal array design as a chemometric method for the optimization of analytical procedures. 5. 3-Level design and its application in microwave dissolution of biological samples, Analyst 120 (4) (1995) 1115–1124.
[30] P.F. Schwarz, et al., A new method to determine the generation of hydroxyl radicals in illuminated TiO_2 suspensions, J. Phys. Chem. B 101 (36) (1997) 7127–7134.
[31] C.S. Turchi, D.F. Ollis, Photocatalytic degradation of organic water contaminants: mechanisms involving hydroxyl radical attack, J. Catal. 122 (1990) 178–192.
[32] K. Ishibashi, et al., Detection of active oxidative species in TiO_2 photocatalysis using the fluorescence technique, Electrochem. Commun. 2 (3) (2000) 207–210.
[33] H.M. Khan, M. Anwar, G. Ahmad, Effect of temperature and light on the response of an aqueous coumarin dosimeter, J. Radioanal. Nucl. Chem. Lett. 200 (6) (1995) 521–527.
[34] G.M. Makrigiorgos, et al., A method for detection of hydroxyl radicals in the vicinity of biomolecules using radiation-induced fluorescence of coumarin, Int. J. Radiat. Biol. 63 (4) (1993) 445–458.
[35] S.C. Ashawa, U.R. Kini, U. Madhvanath, Aqueous coumarin system as a low range chemical dosimeter, Int. J. Appl. Radiat. Isotopes 30 (1) (1979) 7–10.
[36] X.W. Fang, G. Mark, C. vonSonntag, OH radical formation by ultrasound in aqueous solutions. 1. The chemistry underlying the terephthalate dosimeter, Ultrason. Sonochem. 3 (1) (1996) 57–63.
[37] T.J. Mason, et al., Dosimetry in sonochemistry—the use of aqueous terephthalate ion as a fluorescence monitor, Ultrason. Sonochem. 1 (2) (1994) S91–S95.
[38] G.J. Price, E.J. Lenz, The use of dosimeters to measure radical production in aqueous sonochemical systems, Ultrasonics 31 (6) (1993) 451–456.
[39] J.R. McLean, A.J. Mortimer, A cavitation and free-radical dosimeter for ultrasound, Ultrasound Med. Biol. 14 (1) (1988) 59–64.
[40] R.W. Matthews, The radiation-chemistry of the terephthalate dosimeter, Radiat. Res. 83 (1) (1980) 27–41.
[41] J. Haber, et al., Surface-area and porosity, Catal. Today 20 (1) (1994) 11–16.
[42] S. Gregg, K.S.W. Sing, Adsorption, Surface Area and Porosity, Academic Press, New York, 1982.
[43] P.H. Chen, C.H. Jenq, Kinetics of photocatalytic oxidation of trace organic compounds over titanium dioxide, Environ. Int. 24 (8) (1998) 871–879.
[44] S. Qourzal, et al., Photocatalytic degradation and adsorption of 2-naphthol on suspended TiO_2 surface in a dynamic reactor, J. Colloid Interface Sci. 286 (2) (2005) 621–626.
[45] A. Sobczynski, L. Duczmal, Photocatalytic destruction of catechol on illuminated titania, React. Kinet. Catal. Lett. 82 (2) (2004) 213–218.
[46] T.A. McMurray, et al., Intrinsic kinetics of photocatalytic oxidation of formic and oxalic acid on immobilised TiO_2 films, Appl. Catal. A: Gen. 262 (1) (2004) 105–110.
[47] C. Walling, Fentons reagent revisited, Acc. Chem. Res. 8 (4) (1975) 125–131.
[48] S. Goldstein, G. Czapski, J. Rabani, Oxidation of phenol by radiolytically generated $^{\bullet}OH$ and chemically generated $SO_4^{\bullet -}$. A distinction between $^{\bullet}OH$ transfer and hole oxidation in the photolysis of TiO_2 colloid solution, J. Phys. Chem. 98 (26) (1994) 6586–6591.
[49] J. Peral, J. Casado, J. Domenech, Light-induced oxidation of phenol over ZnO powder, J. Photochem. Photobiol. A: Chem. 44 (2) (1988) 209–217.